

# Limb imaging of the Venus O<sub>2</sub> visible nightglow with the Venus Monitoring Camera

A. García Muñoz,<sup>1,2,3</sup> R. Hueso,<sup>4,5</sup> A. Sánchez-Lavega,<sup>4,5</sup> W. J. Markiewicz,<sup>6</sup> D. V. Titov,<sup>1</sup> O. Witasse,<sup>1</sup> and A. Opitz<sup>1,2</sup>

We investigated the Venus O<sub>2</sub> visible nightglow with imagery from the Venus Monitoring Camera on Venus Express. Drawing from data collected between April 2007 and January 2011, we study the global distribution of this emission, discovered in the late 70s by the Venera 9 and 10 missions. The inferred limb-viewing intensities are on the order of 150 kiloRayleighs at the lower latitudes and seem to drop somewhat towards the poles. The emission is generally stable, although there are episodes when the intensities rise up to 500 kR. We compare a set of Venus Monitoring Camera observations with coincident measurements of the O<sub>2</sub> nightglow at 1.27 μm made with the Visible and Infrared Thermal Imaging Spectrometer, also on Venus Express. From the evidence gathered in this and past works, we suggest a direct correlation between the instantaneous emissions from the two O<sub>2</sub> nightglow systems. Possible implications regarding the uncertain origin of the atomic oxygen green line at 557.7 nm are noted.

## 1. Introduction

The Venus atmosphere is a complex chemical system in permanent disequilibrium. Some of the occurring reactions are exothermic and lead to excited-state products that radiate in the form of nightglow. The list of gases contributing to the Venus nightglow includes O, O<sub>2</sub>, NO and OH, which produce emission features throughout the ultraviolet, visible and near-infrared spectrum [Connes *et al.*, 1979; Feldman *et al.*, 1979; García Muñoz *et al.*, 2009a; Krasnopolsky *et al.*, 1977; Piccioni *et al.*, 2008; Slanger *et al.*, 2001].

The Herzberg II system of O<sub>2</sub> is one of such nightglow emissions, resulting from the radiative transition O<sub>2</sub>  $c(0) \rightarrow X(v'') + h\nu$  between 350 and 700 nm. The emission was first detected at Venus by the spectrometers on the Venera 9 and 10 missions [Krasnopolsky *et al.*, 1977] and assigned to the Herzberg II system soon after [Lawrence *et al.*, 1977]. Typically, the emitting layer is ~15–20 km thick

and centered at 90–100 km altitude. Mean values for the overhead intensity are in the range of 2–3 kiloRayleighs (or about 50 times more in limb viewing through the layer center). The Venera spectra did also contain the signature of the O<sub>2</sub> Chamberlain system,  $A'(0) \rightarrow a(v'') + h\nu$ , the ratio of  $c-X$  to  $A'-a$  intensities being about 15 to 1 [Krasnopolsky, 1983]. We refer to the joint emission from the  $c-X$  to  $A'-a$  systems as the Venus O<sub>2</sub> visible nightglow.

There is compelling evidence that the O<sub>2</sub> nightglow [Slanger & Copeland, 2003], including the  $a(0)-X(v''=0, 1)$  bands at 1.27 and 1.58 μm, respectively, arises from one or more O<sub>2</sub><sup>\*</sup> states excited in the three-body reaction:



The oxygen atoms are produced by photodissociation of CO<sub>2</sub> on the planet's dayside and transported to the nightside by subsolar-to-antisolar winds in the upper atmosphere [Fox & Bougher, 1991; Bougher *et al.*, 2006]. In spite of decades of laboratory and planetary (including Earth and Mars) investigations, the understanding of the mechanisms that channel the O<sub>2</sub><sup>\*</sup> product(s) from the reaction of Eq. (1) into the  $c(0)$ ,  $A'(0)$  and  $a(0)$  emitting states remains incomplete.

Indeed, it is remarkable that in the Venus atmosphere the strong O<sub>2</sub>  $a(0)-X(0)$  emission at 1.27 μm (mean overhead intensity of about 1 MR at equatorial latitudes, dropping to ~0.2 MR at 60–70°N, as reported by Piccioni *et al.* [2009] and supported in related work [Drossart *et al.*, 2007; Bailey *et al.*, 2008; Gérard *et al.*, 2009; Soret *et al.*, 2012]) varies locally by more than an order of magnitude on time scales of hours (especially in nadir viewing) [Crisp *et al.*, 1996; Hueso *et al.*, 2008; Piccioni *et al.*, 2009]. However, reported intensities for the O<sub>2</sub> visible nightglow (mostly in limb viewing) fall typically within a range of 2–3 from 150 kR [Krasnopolsky *et al.*, 1977; Bougher & Borucki, 1994; Slanger *et al.*, 2001, 2006, 2012; Gérard *et al.*, 2013; Migliorini *et al.*, 2013].

In the current work, we take a new look at the Venus O<sub>2</sub> visible nightglow by means of imagery of the planet's limb obtained with the Venus Monitoring Camera (VMC) on Venus Express (VEx). The experiment is unique in that it provides snapshot observations over a baseline of nearly four years, longer than past space-based efforts (namely, the Venera 9 and 10 missions, and Pioneer Venus Orbiter, PVO). Unlike PVO, that used the on-board star tracker for monitoring the nightglow [Bougher & Borucki, 1994], VMC provides vertical resolution of the emitting layer. The emerging picture of the Venus O<sub>2</sub> visible nightglow resembles that of the O<sub>2</sub> nightglow at 1.27 μm. A few coincident observations of VMC and the Visible and Infrared Thermal Imaging Spectrometer (VIRTIS, also on VEx) at 1.27 μm support the conclusion. VMC sets a valuable reference for imaging the nightglow on planets other than Earth.

## 2. Selection and treatment of images

VMC is the wide-angle camera on VEx [Markiewicz *et al.*, 2007]. The VMC optical system projects a ~17.5°-field of

<sup>1</sup>ESA/RSSD, ESTEC, 2201 AZ Noordwijk, The Netherlands

<sup>2</sup>ESA Fellow

<sup>3</sup>Grupo de Ciencias Planetarias, Dpto. de Física Aplicada I, ETS Ingeniería, UPV-EHU, Alameda Urquijo s/n, 48013 Bilbao, Spain

<sup>4</sup>Dpto. Física Aplicada I, ETS Ingeniería, UPV-EHU, Alameda Urquijo s/n, 48013 Bilbao, Spain

<sup>5</sup>Unidad Asociada Grupo Ciencias Planetarias UPV/EHU-IAA (CSIC)

<sup>6</sup>Max Planck Institute for Solar System Research, Max-Planck-Str. 2, 37191 Katlenburg-Lindau, Germany

view through four separate spectral channels onto the four quadrants of a CCD detector. The angular resolution is about 0.7 mrad/pixel, which translates into 2.3–5.5 km/pixel at the tangent point for limb viewing and spacecraft planetocentric distances of 7,000–10,000 km. The visible filter is sensitive in the 500–560 nm region, which means it is well suited for detection of the O<sub>2</sub>  $c(0)$ – $X(v''=9, 10)$  bands.

We considered the full public archive of VMC images in the visible channel,<sup>1</sup> which goes from orbits 24 (15/05/2006) to 2099 (18/01/2012). Visual examination of the images including the planet’s limb show a faint though distinct nightglow layer near 100 km altitude when the longest exposure times allowed for by the instrument (30 secs) are utilized. From each image, we obtained 5–6 bins, each bin representing a local time/latitude region on the image, and the corresponding vertical emission profiles. For details on the navigation with the PLIA software [Hueso *et al.*, 2010] and radiometric calibration, see the Supplementary Material. The VMC intensities quoted here refer to the full O<sub>2</sub>  $c(0)$ – $X(v'')$  progression in limb viewing.

We produced a total of 515 bins from 117 images obtained over 38 orbits. The first and last orbits analyzed correspond to numbers 317 and 1716 in the VEx numbering scheme, and date from 04/03/2007 and 01/01/2011, respectively. Solar activity in that period is low, with solar radio fluxes  $F_{10.7\text{cm}}=70$ –90. There are more images probing the northern hemisphere ( $\sim 2/3$  of the total), but overall both hemispheres are comparably well sampled. Often, the images form sequences that probe significant areas of the planet’s nightside in a single orbit. Fig. (I, Top) in the Supplementary Material displays six of those images, exploring the southern hemisphere before periapsis in orbit 1027, whereas Fig. (I, Bottom) shows the range of local times and latitudes probed over the sequence.

Figure (II) in the Supplementary Material shows (black symbols) the local time and latitude at the tangent point for all bins. Latitudes range from 60°S to 65°N and local times are largely (but not exclusively) within two hours from midnight. The red symbols are specific to instances of high nightglow emission. The green and blue symbols represent coincident VMC and VIRTIS observations, respectively. These cases are discussed below.

### 3. Results

Figure (1) shows VMC peak intensities against latitude at the tangent point. The mean limb-viewing intensity in the 20°S–20°N range is  $\sim 150$  kR, which is reasonably consistent with the intensities found by the Veneras [ $\sim(1.5$ – $3) \times 50 = \sim(75$ – $150)$  kR, Krasnopolsky *et al.*, 1977; Krasnopolsky, 1983], PVO [ $\sim(1.5$ – $5.7) \times 50 = \sim(75$ – $285)$  kR, Bougher & Borucki, 1994], VEx/VIRTIS [ $\sim(100$ – $200)$  kR, García Muñoz *et al.*, 2009b; Gérard *et al.*, 2013; Migliorini *et al.*, 2013] and ground-based observations [ $\sim(3$ – $5) \times 50 = \sim(150$ – $250)$  kR, Slanger *et al.*, 2001, 2006]. For reference, the figure includes the average intensities from 90 to 100 km altitude for both the visible and near-infrared emissions as measured with VIRTIS between January 2007 and May 2008 [García Muñoz *et al.*, 2009b]. The latter are scaled by an estimated ratio for the visible and near-infrared emissions of 1/200. The VIRTIS data conform to the canonical view that the O<sub>2</sub> nightglow peaks near the antisolar point because the recombining oxygen atoms are transported from the dayside in the subsolar-to-antisolar circulation pattern [Bougher *et al.*, 2006; Brecht *et al.*, 2011].

Our interpretation of Fig. (1) is that the VMC intensities generally decay with latitude, a view that follows that for the averaged VIRTIS data. The conclusion is more easily justified for the southern hemisphere, but is also consistent

with a large number of the VMC measurements over the northern hemisphere. Thus, the dispersion in the VMC intensities, particularly north of 40°N, likely reflects temporal and spatial variations, such as those known to occur at 1.27  $\mu\text{m}$ . A few brighter-than-average episodes are found in orbits 352, 364 and 1286 (see Fig. II, red symbols), having peak intensities that reach above 350 kR, which has an impact on the trend of VMC points in Fig. (1).

The lack of symmetry between the two hemispheres, even in the instances of moderate emission, may be caused by the different vertical resolution in the measurements north and south of the equator. The VEx orbit imposes that the VMC spatial resolution at the limb improves as the spacecraft nears the northern polar latitudes, which leads to a progressive positive bias in the corresponding peak intensities.

The optical axes of both the VMC and VIRTIS instruments are aligned along the +z-axis of VEx, which makes it possible to obtain simultaneous, co-located observations of the Venus atmosphere. We identified four orbits (317, 360, 600 and 602) for which we can directly compare the O<sub>2</sub> visible nightglow, as observed with VMC, and the O<sub>2</sub> near-infrared nightglow, as observed with VIRTIS. Table (1) summarizes some relevant information about the VMC bins in those orbits. Figure (2) shows the two sets of intensities against latitude, with green and blue symbols representing VMC and VIRTIS data, respectively. Local times and latitudes specific to the VMC and VIRTIS observations in the four orbits are shown in Fig. (II). Both sets of intensities appear reasonably consistent, especially where the two instruments probe overlapping regions (i.e., orbits 317, 600, 602). Orbit 602 exhibits moderate enhancements in the two emissions, when the VMC intensities reach 250–300 kR. The comparison would obviously benefit from a longer record of simultaneous measurements, especially if conditions of high emission could be identified.

Figure (3, Left) shows the emission vertical profiles for VMC and VIRTIS data in a few selected examples from orbit 600. The VMC profiles are visibly broader than the VIRTIS ones, which likely results from three factors specific to VMC, namely its poorer spatial resolution (the VIRTIS instantaneous field of view is  $2.5 \times 10^{-4}$  rad/pixel), the co-addition of vertical profiles obtained with relatively long exposure times, and a point spread function of a few pixels [Titov *et al.*, 2012]. It is difficult to estimate the accuracy in the absolute vertical scale of the VMC profiles and, thus, we have focused on the magnitudes of the emission peaks. Uncertainty bars for the intensities are given for one VMC profile. They are calculated, at each altitude, as the standard deviation of the intensity from profiles that contribute to the bin. The uncertainty bars are affected by the three factors mentioned above, but they also provide a measure of the photon statistics and the spatial variability of the nightglow emission within the bin. The intensities and uncertainty bars shown in Figs. (1)–(2) are specific to the altitude of peak emission.

Nightglow observations may be used for remotely sensing the atmospheric atomic oxygen. As a demonstration, we retrieved the atom number densities for the three VMC emission profiles in Fig. (3, Left) with the energy-transfer parameters for excitation and quenching of the Venus O<sub>2</sub> visible nightglow derived by García Muñoz *et al.* [2009b]. The profiles are plotted in Fig. (3, Right), and show atomic oxygen number densities of  $10^{11}$ – $10^{12}$  cm<sup>-3</sup> at 100 km. Such values are somewhat larger than, but in reasonable agreement with, the retrievals from the O<sub>2</sub> nightglow at 1.27  $\mu\text{m}$  [García Muñoz *et al.*, 2009b; Gérard *et al.*, 2009] at the same altitude. The broad emission profiles lead to somewhat over-estimated atomic oxygen number densities at the higher altitudes.

## 4. Discussion

The VMC observations analyzed here show that the O<sub>2</sub> visible nightglow is a permanent feature of the Venus night-side. The intensities seem to peak at low latitudes and drop polewards, which is consistent with past O<sub>2</sub> visible and near-infrared nightglow observations with VIRTIS [García Muñoz et al., 2009b]. The nightglow is variable, as demonstrated by occasional high emission events.

The main conclusion is that the O<sub>2</sub> visible nightglow resembles the O<sub>2</sub> nightglow at 1.27 μm. This suggests, in turn, a direct correlation between the two, which is not unexpected since both emissions can ultimately be traced to the recombination reaction of Eq. (1). In this respect, we note the importance of the viewing geometry when comparing various measurements. Most pre-VEx observations of the O<sub>2</sub> nightglow at 1.27 μm came from nadir observations [Bailey et al., 2008; Connes et al., 1979; Crisp et al., 1996, e.g.]. However, pre-VEx space-based observations of the O<sub>2</sub> visible nightglow were typically conducted in limb viewing [Krasnopolsky et al., 1977; Bougher & Borucki, 1994], which tends to smooth out localized features and therefore minimize changes.

The tentative correlation may bear implications for the excitation of the atomic oxygen green line at 557.7 nm [Slanger et al., 2001]. By now, the green line has been detected several times, always from the ground [Slanger et al., 2006, 2012; Gray et al., 2012], its intensity being permanently more than tenfold fainter than the 170 R of overhead intensity on the occasion of its discovery. We cannot prove a connection between the O<sub>2</sub> visible nightglow and the green line (such a connection would hint at a mesospheric origin of the latter), and cannot either explain why the overhead intensity for the O<sub>2</sub> c-X system was relatively normal (5.1 kR, i.e. about 250 kR in limb viewing) on the occasion of the Venus green line discovery. However, it appears that the O<sub>2</sub> visible nightglow may be as variable as the associated emission at 1.27 μm. A usual objection for the green line originating in the mesosphere in the interaction with an energetic O<sub>2</sub> precursor state is that the relatively energetic O<sub>2</sub> c(0) state was considered to undergo little variability. The realisation that the O<sub>2</sub> visible nightglow may be as variable as the near-infrared emission eliminates a fundamental impediment to a mesospheric origin of the atomic oxygen green line. The realisation, however, is not sufficient to prove a direct connection between the O<sub>2</sub> and O nightglow emissions or to rule out the other mesospheric and ionospheric mechanisms for excitation of the green line proposed in recent years [Slanger et al., 2006, 2012; Fox, 2012].

**Acknowledgments.** RH and ASL were supported by the Spanish MICINN project AYA2009-10701 and AYA2012-36666 with FEDER support, Grupos Gobierno Vasco IT-464-07 and UPV/EHU UFI11/55. AGM gratefully acknowledges the assistance of Teresa del Río-Gaztelurrutia (UPV/EHU, Bilbao, Spain) with PLIA.

## Notes

1. <ftp://psa.esac.esa.int/pub/mirror/VENUS-EXPRESS/VMC/>

## References

- Bailey, J., V.S. Meadows, S. Chamberlain, and D. Crisp (2008), The temperature of the Venus mesosphere from O<sub>2</sub>(a<sup>1</sup>Δ<sub>g</sub>) airglow observations, *Icarus*, 197, 247–259.
- Bougher, S.W., S. Rafkin, and P. Drossart (2006), Dynamics of the Venus upper atmosphere: Outstanding problems and new constraints expected from Venus Express, *Planet. Space Sci.*, 54, 1,371–1,380.
- Bougher, S.W., and W.J. Borucki (1994), Venus O<sub>2</sub> visible and IR nightglow: Implications for lower thermosphere dynamics and chemistry, *J. Geophys. Res.*, 99, 3,759–3,776.
- Brecht, A.S., S.W. Bougher, J.-C. Gérard, C.D. Parkinson, S. Rafkin, and B. Foster (2011), Understanding the variability of nightside temperatures, NO UV and O<sub>2</sub> IR nightglow emissions in the Venus upper atmosphere, *J. Geophys. Res.*, 116, E08004, doi:10.1029/2010JE003770.
- Connes, P., J.F. Noxon, W.A. Traub, and P. Carleton (1979), O<sub>2</sub>(<sup>1</sup>Δ) emission in the day and night airglow of Venus, *Astrophys. J.*, 233, L29–L32.
- Crisp, D., V.S. Meadows, B. Bézard, C. de Bergh, J.-P. Maillard, and F.P. Mills (1996), Ground-based near-infrared observations of the Venus nightside: 1.27-μm O<sub>2</sub>(a<sup>1</sup>Δ<sub>g</sub>) airglow from the upper atmosphere, *J. Geophys. Res.*, 101, E2, 4,577–4,594.
- Drossart, P., G. Piccioni, J.-C. Gérard, M.A. Lopez-Valverde, A. Sanchez-Lavega, et al. (2007), A dynamic upper atmosphere of Venus as revealed by VIRTIS on Venus Express, *Nature*, 450, 641–645.
- Feldman, P.D., H.W. Moos, J.T. Clarke, and A.L. Lane (1979), Identification of the UV nightglow from Venus, *Nature*, 279, 221–222.
- Fox, J.L., and S.W. Bougher (1991), Structure, luminosity, and dynamics of the Venus thermosphere, *Space Sci. Rev.*, 55, 357–489.
- Fox, J.L. (2012), The ionospheric source of the red and green lines of atomic oxygen in the Venus nightglow, *Icarus*, 221, 787–799.
- García Muñoz, A., F.P. Mills, G. Piccioni, and P. Drossart (2009a), The near-infrared nitric oxide nightglow in the upper atmosphere of Venus, *Proc. Natl. Acad. Sci. U.S.A.*, 106, 985–988.
- García Muñoz, A., F.P. Mills, T.G. Slanger, G. Piccioni, and P. Drossart (2009b), Visible and near-infrared nightglow of molecular oxygen in the atmosphere of Venus, *J. Geophys. Res.*, 114, E12002, doi:10.1029/2009JE003447.
- Gérard, J.-C., A. Saglam, G. Piccioni, P. Drossart, F. Montmessin, and J.-L. Bertaux (2009), Atomic oxygen distribution in the Venus mesosphere from observations of O<sub>2</sub> infrared airglow by VIRTIS-Venus Express, *Icarus*, 199, 264–272.
- Gérard, J.-C., L. Soret, A. Migliorini, and G. Piccioni (2013), Oxygen nightglow emissions of Venus: Vertical distribution and collisional quenching, *Icarus*, 223, 602–608.
- Gray, C. L., N. Chanover, and T. Slanger (2012), Coronal mass ejections and their effect on the Venusian nightglow, American Geophysical Union, Fall Meeting.
- Hueso, R., A. Sánchez-Lavega, G. Piccioni, P. Drossart, J.C. Gérard, et al. (2008), Morphology and dynamics of Venus oxygen airglow from Venus Express/Visible and Infrared Thermal Imaging Spectrometer observations, *J. Geophys. Res.*, 113, E00B02, doi:10.1029/2008JE003081.
- Hueso, R., J. Legarreta, J.F. Rojas, J. Peralta, S. Pérez-Hoyos, T. del Río-Gaztelurrutia, and A. Sánchez-Lavega (2010), The Planetary Laboratory for Image Analysis (PLIA), *Adv. Space Res.*, 46, 1,120–1,138.
- Krasnopolsky, V.A. (1983), Venus spectroscopy in the 3000–8000 Å region by Veneras 9 and 10, in *Venus*, edited by D.M. Hunten et al., pp. 459–483, Univ. of Ariz., Press, Tucson.
- Krasnopolsky, V.A., A.A. Krysko, V.N. Rogachev, and V.A. Parshv (1977), Spectroscopy of the night-sky luminiscence of Venus from the interplanetary spacecraft Venera 9 and Venera 10, *Cosmic Res.*, Engl. Transl., 14, 687–692.
- Lawrence, G.M., C.A. Barth, and V. Argabright (1977), Excitation of the Venus night airglow, *Science*, 195, 573–574.
- Markiewicz, W.J., D.V. Titov, N. Ignatiev, H.U. Keller, D. Crisp, et al. (2007), Venus Monitoring Camera for Venus Express, *Planet. Space Sci.*, 55, 1,701–1,711.
- Migliorini, A., A. Piccioni, J.-C. Gérard, L. Soret, T.G. Slanger, R. Politi, M. Snels, and P. Drossart (2013), The characteristics of the O<sub>2</sub> Herzberg II and Chamberlain bands observed with VIRTIS/Venus Express, *Icarus*, 223, 609–614.
- Piccioni, G., P. Drossart, L. Zasova, A. Migliorini, J.-C. Gérard, et al. (2008), First detection of hydroxyl in the atmosphere of Venus, *A. & A. Lett*, 483, L29–L33.

**Table 1.** Image number, local time (LT), latitude (Lat), peak intensity ( $I_{\text{peak}}$ ) and altitude at the intensity peak ( $z_{\text{peak}}$ ) for selected VMC bins in orbits 317, 600 and 602, for which there are simultaneous VIRTIS observations.

Image	LT	Lat	$I_{\text{peak}}$ [kR]	$z_{\text{peak}}$ [km]
317_89	24.6	63.7	101.3	93
317_89	24.5	60.8	142.3	95
317_89	24.3	57.9	145.9	100
317_90	24.6	63.6	149.8	97
317_90	24.5	62.3	143.2	99
600_98	23.1	59.4	217.0	94
600_98	23.2	57.0	278.4	98
600_98	23.2	54.6	244.7	97
602_175	23.5	43.9	182.4	101
602_175	23.5	41.4	132.8	98
602_175	23.5	39.0	150.7	90
602_176	23.3	59.3	121.9	93
602_176	23.4	56.6	157.3	95
602_176	23.5	53.7	115.4	96

Piccioni, G., L. Zasova, A. Migliorini, P. Drossart, A. Shakun, et al. (2009), Near-IR oxygen nightglow observed by VIRTIS in the Venus upper atmosphere, *J. Geophys. Res.*, *114*, E00B38, doi:10.1029/2008JE003133.

Slanger, T.G., P.C. Cosby, D.L. Huestis, and T.A. Bida (2001), Discovery of the atomic oxygen green line in the Venus night airglow, *Science*, *291*, 463–465.

Slanger, T.G., and R.A. Copeland (2003), Energetic oxygen in the atmosphere and in the laboratory, *Chem. Rev.*, *103*, 4731–4766.

Slanger, T.G., D.L. Huestis, P.C. Cosby, N.J. Chanover, and T.A. Bida (2006), The Venus nightglow: Ground-based observations and chemical mechanisms, *Icarus*, *182*, 1–9.

Slanger, T.G., N.J. Chanover, B.D. Sharpee, and T.A. Bida (2012), O/O<sub>2</sub> emissions in the Venus nightglow, *Icarus*, *217*,

845–848.

Soret, L., J.-C. Gérard, F. Montmessin, G. Piccioni, P. Drossart, and J.-L. Bertaux (2012), Atomic oxygen on the Venus night-side: Global distribution deduced from airglow mapping, *Icarus*, *217*, 849–855.

Svedhem, H., D.V. Titov, F.W. Taylor, and O. Witasse (2007), Venus as a more Earth-like planet, *Nature*, *450*, 629–632.

Titov, D.V., W.J. Markiewicz, N.I. Ignatiev, L. Song, S.S. Limaye, A. Sánchez-Lavega, et al. (2012), Morphology of the cloud tops as observed by the Venus Express Monitoring Camera, *Icarus*, *217*, 682–701.

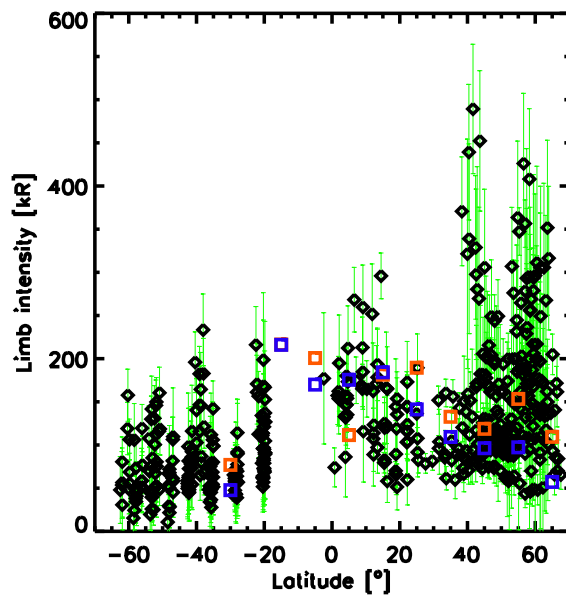


**Figure 1.** Black diamonds: Limb-integrated intensity against latitude for the full set of analyzed VMC bins. The uncertainty bars are standard deviations in the intensity at the altitude of the emission peak (see text and Fig. (3)). Blue squares: VIRTIS limb-integrated intensity (scaled by 1/200) for the O<sub>2</sub> a(0)-X(0) band at 1.27 μm as published in *García Muñoz et al.* [2009b]. Red squares: VIRTIS limb-integrated intensity for the O<sub>2</sub> visible nightglow.

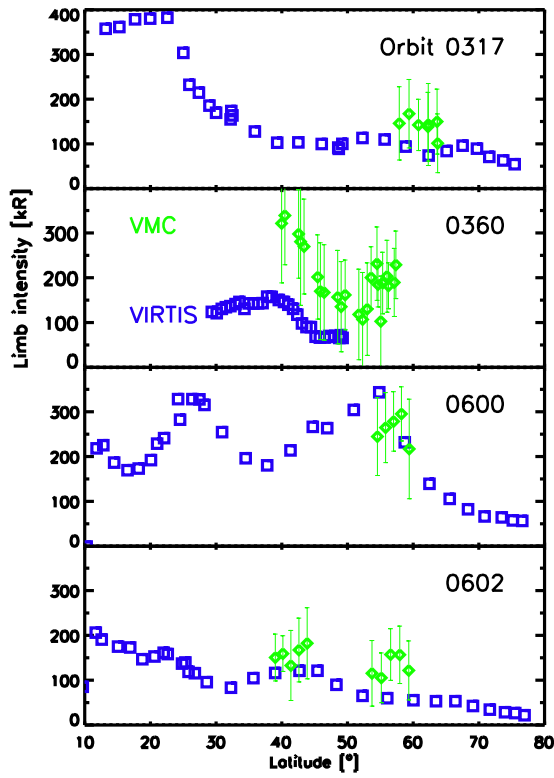


**Figure 2.** Limb-integrated intensity against latitude for orbits 317, 360, 600 and 602. Green diamonds: VMC observations, and associated uncertainties. Blue squares: Coincident VIRTIS observations of the O<sub>2</sub>  $a(0)$ – $X(0)$  band at 1.27  $\mu\text{m}$  (scaled by 1/200). Uncertainties in the VIRTIS measurements are less than for VMC, and therefore omitted.

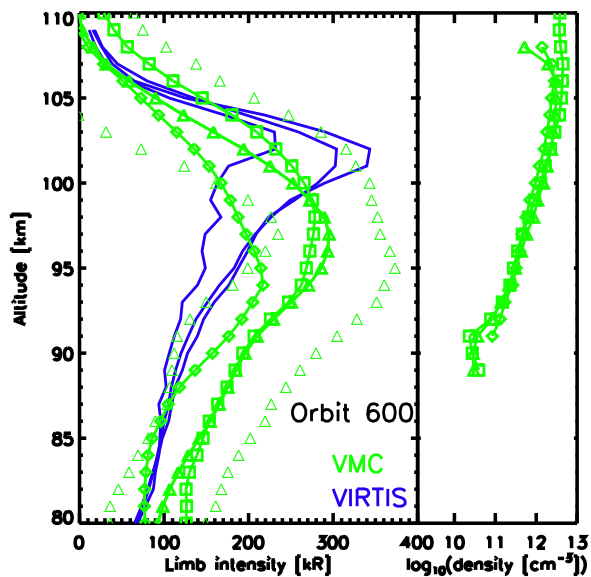


**Figure 3.** Left. Limb-integrated intensity against tangent altitude for three bins from orbit 600 (thick triangles, squares and diamonds), where intensities are relatively high. Each bin corresponds to a slightly different latitude, as seen in Fig. (2). Both VMC profiles of the O<sub>2</sub> visible nightglow and VIRTIS profiles of the O<sub>2</sub>  $a(0)$ – $X(0)$  band at 1.27  $\mu\text{m}$  (scaled by 1/200) are shown. Uncertainties at each altitude are given for the VMC profile with triangle symbols and shown with disconnected triangles. For any one bin, the uncertainties given in Figs. (1) and (2) are the uncertainties at the altitude of peak emission of the corresponding profile. The mismatch in the altitude of the visible and near-infrared emission peaks is likely affected by the different integration times and spatial resolutions of the two instruments. Right. Atomic oxygen profiles retrieved from the VMC profiles on the left panel.